
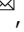




Declining nutrient availability and metal pollution in the Red Sea

Chunzhi Cai ¹, Antonio Delgado Huertas ² & Susana Agusti ¹

Reconstructing sediment accumulation rates reveals historical environmental shifts. We analyzed 15 element concentrations and accumulation rates in two Red Sea sediment cores over 500 years. Post-1870s, the South Red Sea experienced a significant drop in element accumulation rates, with a noticeable decline in nutrients like magnesium (−8.52%), organic carbon (−14.9%), nitrogen (−14.0%), phosphorus (−16.4%), sulfur (−17.2%), and calcium (−17.8%). This suggests a potential reduction in nutrient inflow from the Indian Ocean, possibly due to warming-induced ocean stratification. Conversely, the North Red Sea saw an increase in all element accumulation rates after the 1870s, highlighting a rise in trace elements such as iron (4.56%), cadmium (8.69%), vanadium (12.6%), zinc (13.8%), copper (14.4%), chromium (17.6%), and nickel (19.5%), indicative of increased anthropogenic coastal activities. We introduce the term “Cai-Agusti Marine Crisis Conflux” to encapsulate the escalating thermal stress, nutrient depletion, and elemental pollution in the Red Sea, underscoring potential risks to its ecosystems and global implications.

¹King Abdullah University of Science and Technology, Red Sea Research Center, Biological and Environmental Sciences and Engineering Division, Thuwal 23955, Kingdom of Saudi Arabia. ²Instituto Andaluz de Ciencias de la Tierra, CSIC-UGR, Armilla, Spain. ✉email: chunzhi.cai@kaust.edu.sa

Over the past two centuries, human activities, such as industrialization, urbanization, globalization, and population growth, have irrefutably altered the Earth's geological history, leading to substantial chemical disruptions and the onset of global climate change, including global warming¹. By reconstructing element concentrations and accumulation rates in natural archives, such as ice cores and sediment records, we can gain a unique insight into how humans have responded to these challenges and predict the potential influence of these changes on the future².

The Red Sea is a subtropical oligotrophic sea. Its nutrient sources primarily depend on vertical mixing in the northern region and wind-induced horizontal intrusion of nutrient-rich waters from the Indian Ocean in the southern region³. However, due to its semi-enclosed nature, infrequent precipitation, lack of riverine inputs, and hot climate, the Red Sea is considered one of the warmest sea basins globally, making it highly susceptible to warming^{4,5}. Additionally, the Red Sea serves as a natural analog for potential future scenarios of overheated seas in the context of global warming.

Recent studies have revealed that the maximum surface temperatures of the Red Sea have been increasing at an alarming rate of 0.17 ± 0.07 °C per decade, surpassing the global ocean warming rate of 0.11 °C per decade⁴. This rapid warming has already led to anomalous heat waves and severe coral bleaching events^{6,7}. Moreover, the warming trend is anticipated to exacerbate the severity of ocean stratification, impeding vertical exchanges between the surface and deep water layers, and curtailing nutrient availability for primary production, ultimately leading to food shortages for fish and other marine organisms^{8–11}. It can also influence the interchange of water with the Indian Ocean^{12,13}.

In addition to warming, the Red Sea is susceptible to various anthropogenic disturbances, including trace metal pollution^{14–16}. The opening of the Suez Canal in 1869 coincided with the beginning of the Second Industrial Revolution between 1870 and

1914. This event, along with the discovery of the first Saudi Arabian oil field in 1938, contributed to a surge in commercial and oil shipping activities¹⁷, extensive development of oil-related industries¹⁸, and rapid urbanization and population growth in coastal cities along the Red Sea. These human activities may have released considerable amounts of trace metals into the Red Sea.

Sediment cores serve as the ultimate repository of trace metals in aquatic environments, offering a historical record of environmental changes and human influence over extended periods¹⁹. In the Red Sea, where riverine inputs are absent, and precipitation/runoff is negligible, sediment cores provide a clear and decipherable historical record. However, despite this potential, few studies have reported element concentrations in Saudi Arabian Red Sea sediment cores^{20–23}, with most studies focused on coastal sediments and lacking supplemental chronological analysis. Thus, the spatial and temporal variability of element concentrations in the open Red Sea remains largely unknown.

The study examines the spatial and temporal variability of the 15 most representative elements in sediment cores collected from the North and South open Red Sea over the past centuries. The study determines whether the observed variations are due to natural forces or anthropogenic activities. The primary aim of this research is to establish a robust baseline for evaluating the long-term effects of human activities on marine environments, locally and globally. Additionally, the study aims to provide policy-makers with targeted mitigation strategies to preserve and protect the fragile marine ecosystem in the Red Sea.

Results and Discussion

Declining nutrient input from the Indian Ocean to the Red Sea. The chronological analyses indicate that the dates of sediment cores range from the 1590s to the 2010s. The spatial and temporal changes in 15 element concentrations in the Red Sea sediment cores are ranked in descending order by their mean values as follows: calcium (Ca) > silica (Si) > total organic carbon

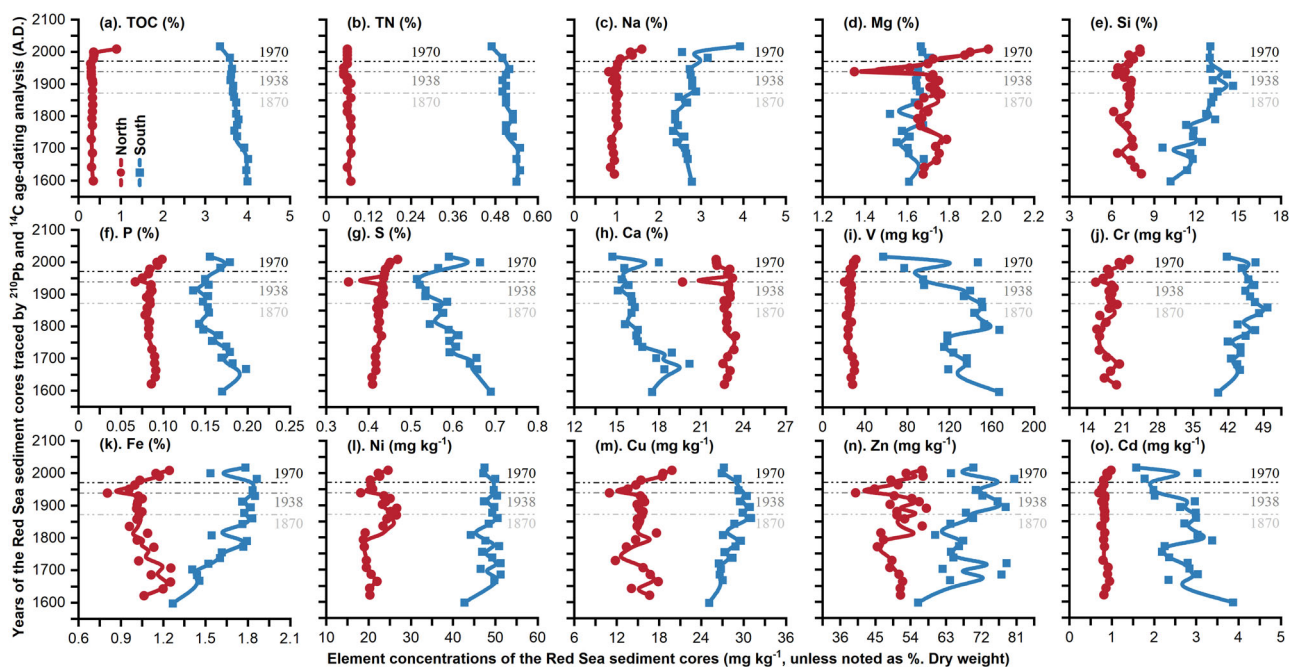


Fig. 1 Scatter plots of element concentrations in the Red Sea sediment cores. **a–o** Total organic carbon (TOC), total nitrogen (TN), Na, Mg, Si, P, S, Ca, V, Cr, Fe, Ni, Cu, Zn, and Cd concentrations (mg kg^{-1} , unless noted as %, which is equal to $10,000 \text{ mg kg}^{-1}$, dry-weight basis) in sediment cores collected from the South (blue lines and squares, $N = 20$) and North (red lines and circles, $N = 25$) Red Sea. Smooth lines were constructed using the adjacent-averaging method using OriginPro 2022 software.

Table 1 Average element concentrations of the Red Sea sediment cores.

Element	South Red Sea (N = 20)	North Red Sea (N = 25)	South & North Red Sea (N = 45)
Ca (%)	16.7 ± 1.39 (14.7–20.2) B	22.7 ± 0.72 (19.7–23.5) A	20.0 ± 3.21 (14.7–23.5)
Si (%)	12.5 ± 1.26 (9.62–14.6) A	7.21 ± 0.51 (6.16–8.11) B	9.49 ± 2.80 (6.16–14.6)
TOC (%)	3.71 ± 0.16 (3.35–4.01) A	0.35 ± 0.13 (0.29–0.90) B	1.90 ± 1.70 (0.29–4.01)
Na (%)	2.71 ± 0.35 (2.34–3.92) A	1.03 ± 0.17 (0.82–1.60) B	1.77 ± 0.88 (0.82–3.92)
Mg (%)	1.64 ± 0.047 (1.52–1.71) B	1.72 ± 0.11 (1.35–1.99) A	1.68 ± 0.10 (1.35–1.99)
Fe (%)	1.66 ± 0.18 (1.27–1.86) A	1.07 ± 0.10 (0.80–1.26) B	1.33 ± 0.33 (0.80–1.86)
S (%)	0.59 ± 0.050 (0.51–0.69) A	0.43 ± 0.02 (0.35–0.47) B	0.50 ± 0.09 (0.35–0.69)
TN (%)	0.52 ± 0.020 (0.47–0.55) A	0.060 ± 0.0060 (0.050–0.071) B	0.27 ± 0.23 (0.050–0.55)
P (%)	0.16 ± 0.016 (0.14–0.20) A	0.090 ± 0.0060 (0.067–0.099) B	0.12 ± 0.040 (0.067–0.20)
V (mg kg ⁻¹)	127 ± 28.8 (57.3–167) A	26.7 ± 2.47 (21.0–31.5) B	71.4 ± 54.0 (21.0–167)
Zn (mg kg ⁻¹)	68.8 ± 6.70 (56.0–80.5) A	50.9 ± 4.34 (39.9–58.1) B	58.9 ± 10.5 (39.9–80.5)
Ni (mg kg ⁻¹)	48.5 ± 2.29 (42.7–51.3) A	22.1 ± 2.54 (18.2–26.7) B	33.8 ± 13.5 (18.2–51.3)
Cr (mg kg ⁻¹)	45.1 ± 2.43 (40.0–49.8) A	18.5 ± 1.62 (15.7–22.4) B	30.3 ± 13.5 (15.7–49.8)
Cu (mg kg ⁻¹)	28.3 ± 1.66 (25.1–31.1) A	15.6 ± 2.02 (11.0–19.9) B	21.2 ± 6.66 (11.0–31.1)
Cd (mg kg ⁻¹)	2.64 ± 0.57 (1.58–3.87) A	0.84 ± 0.06 (0.70–0.99) B	1.64 ± 0.98 (0.70–3.87)

TOC total organic carbon, TN total nitrogen.

Notes: Mean ± standard deviation, minimum and maximum in parentheses, mg kg⁻¹, unless noted as %, which is equal to 10,000 mg kg⁻¹, dry-weight basis of the South and North Red Sea sediment cores. Data in the same row marked with different letters are significantly different (*p* < 0.05).

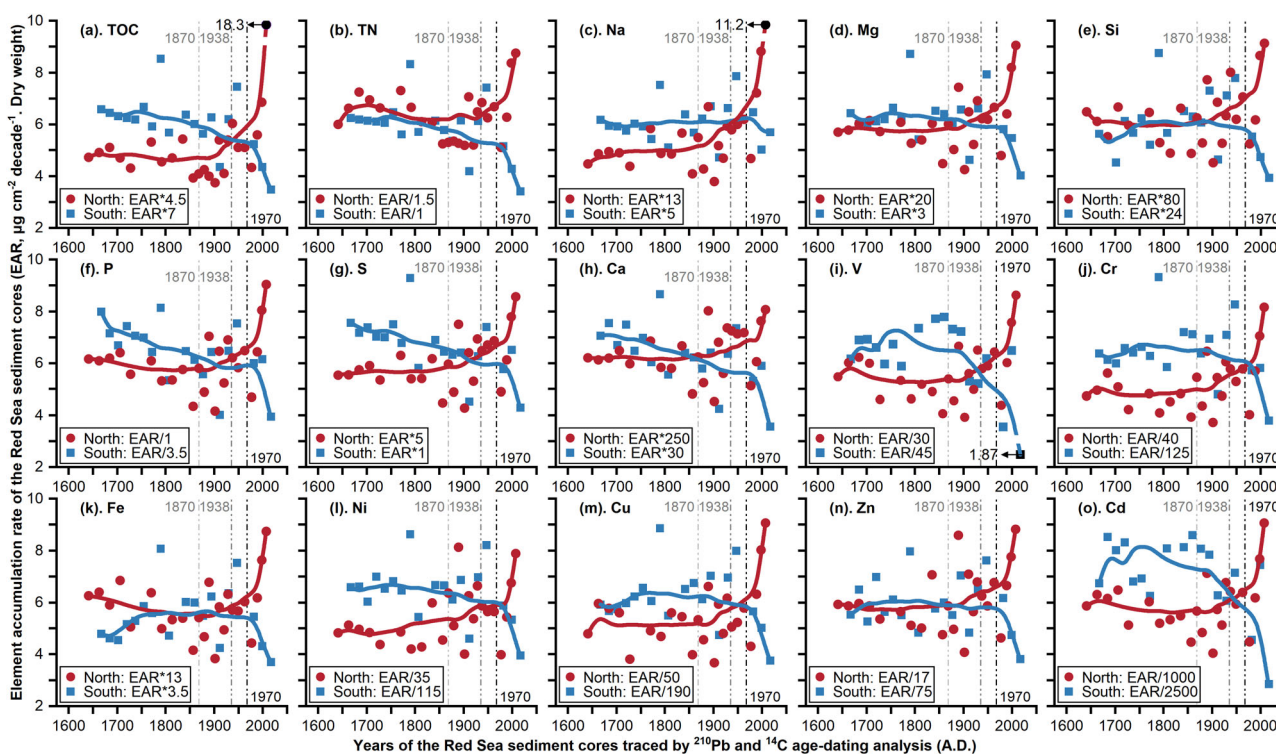


Fig. 2 Scatter plots of element accumulation rates in the Red Sea sediment cores. a–o, Total organic carbon (TOC), total nitrogen (TN), Na, Mg, Si, P, S, Ca, V, Cr, Fe, Ni, Cu, Zn, and Cd element accumulation rates (EAR, $\mu\text{g cm}^{-2} \text{decade}^{-1}$, dry weight) in sediment cores collected from the South (blue lines and squares, *N* = 19) and North (red lines and circles, *N* = 24) Red Sea. The EAR data were standardized and presented in different orders of magnitude for comparison, as noted in each legend. The accumulation rates of TOC, Na, Mg, Si, S, Ca, and Fe were multiplied by a factor ranging from 1 to 250, whereas those of TN, P, V, Cr, Ni, Cu, Zn, and Cd were divided by a factor ranging from 1 to 1/2500. Values below or above the y-axis scale are labeled and highlighted with a black symbol. Smooth lines were constructed using the adjacent-averaging method using OriginPro 2022 software.

(TOC) > sodium (Na) > magnesium (Mg) > iron (Fe) > sulfur (S) > total nitrogen (TN) > phosphorus (P) > vanadium (V) > zinc (Zn) > nickel (Ni) > chromium (Cr) > copper (Cu) > cadmium (Cd). Further statistical analysis revealed that the South Red Sea sediment cores exhibited significantly higher element concentrations (excluding Ca and Mg; Table 1) but remarkably lower element accumulation rates (EARs, excluding TOC and TN, Fig. 2, Supplementary Table 1) compared to those of the North Red Sea (*p* < 0.01).

Although Cd is not commonly known as a required nutrient for organisms, it is a bioactive trace element^{24,25} that can effectively stimulate the growth of marine phytoplankton in seawater with depleted Zn²⁶. This study found that Cd concentrations in South Red Sea sediment cores were positively correlated with nutrient element concentrations, such as TOC, TN, and P (*R* values > 0.58, *p* < 0.01; Fig. 3a), and were higher than in the North Red Sea (Table 1). This finding is consistent with a previous study on the Red Sea zooplankton¹⁵, which

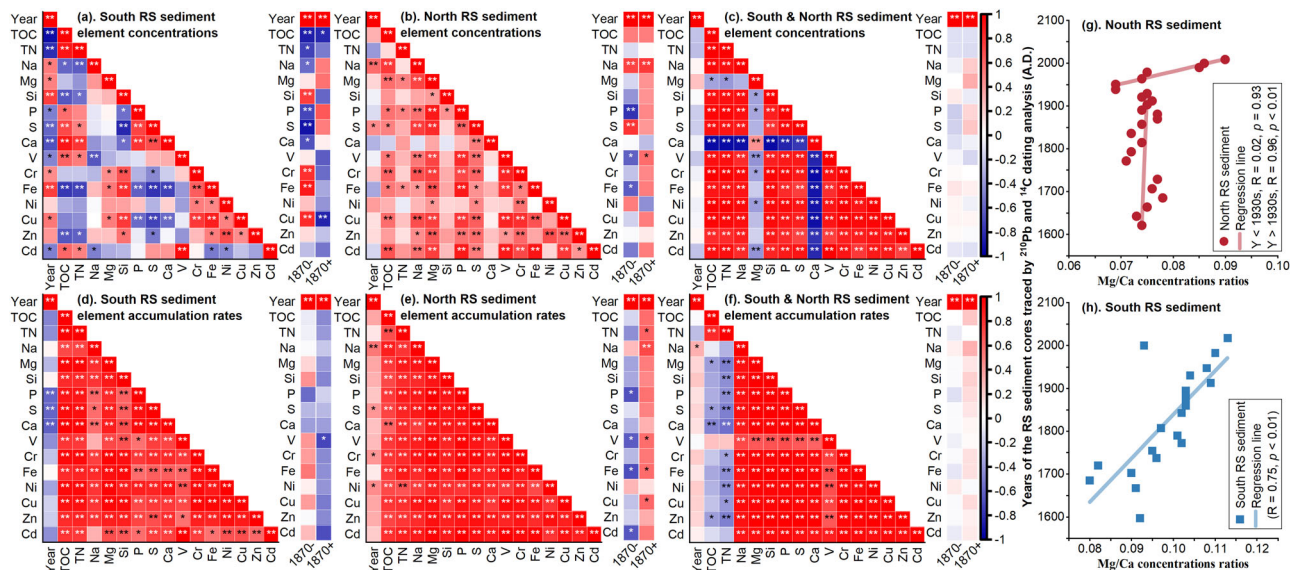


Fig. 3 Heatmaps of Pearson correlations among age, elemental concentrations, and accumulation rates; scatter plot of Mg/Ca ratios vs. age in Red Sea sediment cores. **a–c** Heatmaps of the Pearson correlation coefficients between chronological age (years, marked as 1870– and 1870+ for before and after the 1870s), 15 elemental concentrations, and **d–f** 15 element accumulation rates of the sediment cores collected from South, North, and both regions of the Red Sea (RS). * $p < 0.05$, ** $p < 0.01$. Scatter plot of the linear regression between Mg/Ca concentration ratios and chronological age (years, abbreviated Y in the legend) of the **g**, North (red lines and circles, $N = 25$), and **h**, South (blue lines and squares, $N = 20$) Red Sea sediment core.

reported higher nutrient element concentrations (e.g., TOC, TN, and P) in zooplankton samples collected in the South Red Sea compared to the central and northern Red Sea and positive correlations with Cd.

The analysis suggests that nutrients in the Red Sea originate from the Indian Ocean, with their concentrations decreasing at a gradient toward the North due to the semi-enclosed structure of the Red Sea, the absence of riverine inputs, and the negligible precipitation/runoff. This finding is supported by previous studies^{5,12,13} that the nutrient sources of the oligotrophic Red Sea rely primarily on the horizontal intrusion (wind-induced) of nutrient-rich waters from the Indian Ocean through the Gulf of Aden. Furthermore, the data reveal significantly higher trace metal concentrations, such as V, Cr, Fe, Ni, Cu, Zn, and Cd, in the South Red Sea sediment cores ($p < 0.05$, Table 1). These results suggest that the Indian Ocean is a nutrient supplier and an important source of trace metals to the Red Sea.

Since the onset of the Second Industrial Revolution, the mean accumulation rates of various nutrient elements, including TOC (-14.9%), TN (-14.0%), P (-16.4%), S (-17.2%), and Cd (-23.0%), have notably decreased in the South Red Sea sediment core. Moreover, the decline rate increased significantly after the 1970s, as depicted in Figs. 2 and 3e and Table 2. The linear regression slopes between the TOC, TN, and Cd element accumulation rates and the years before and after 1870 have decreased remarkably by 2.79, 2.93, and 5.54 times, respectively (Table 3). These findings indicate that the Red Sea received fewer nutrients from the Indian Ocean at an accelerating pace after the 1870s and 1970s. The reduction in nutrient supplies may potentially be attributed to the rapid warming and enhanced ocean stratification over the Indian Ocean^{27,28} and the Red Sea^{4,5} over the past 150 years, as a result of increasing greenhouse gas emissions worldwide²⁹. Notably, organisms recycle both Cd and P, and the ratio of dissolved Cd/P concentrations in the Indian Ocean was observed to increase with depth³⁰. Our findings indicated a notable reduction in Cd/P concentration ratios in sediments from the South Red Sea post-1800s (Supplementary Fig. 1, Supplementary Data 2). This reduction could imply a more frequent utilization of surface

waters by organisms or a diminished upwelling of water from the Indian Ocean into the South Red Sea. Intriguingly, this trend seems to have manifested possibly before the onset of the Second Industrial Revolution (~1870s).

Sediment Mg/Ca concentration ratios have been widely employed to reconstruct past sea surface temperatures (SSTs) in tropical oceans where instrumental data are limited³¹. As per thermodynamic laws, higher seawater temperatures favor the substitution of Mg for Ca in carbonate sediments³². The current study found a significant change in the Mg/Ca ratio in the South Red Sea during the end of the Little Ice Age, followed by a less steep trend that has continued since the industrial revolution (Fig. 3h). In the North Red Sea, a drastic change occurred in the last 70 years, coinciding with the increase in oil exploitation (local effects) and acceleration of global change effects (Fig. 3g; Supplementary Data 3).

The Mg/Ca concentration ratios in the South Red Sea have a positive correlation with time (R -value = 0.75, $p < 0.01$, Fig. 3h), indicating a considerable increase in SSTs in the South Red Sea in the past few centuries. This hypothesis aligns with a previous study³³ that global temperatures have steadily risen since the end of the Little Ice Age for 200 years. Furthermore, it is noteworthy that the warm pool areas in the tropical Indian Ocean, characterized by SSTs exceeding 28 °C and holding a direct connection to the South Red Sea through the Gulf of Aden, have undergone a rapid expansion over the last 150 years²⁸.

As global warming continues and sea levels rise, the Indian Ocean may expand, leading to an increased flow of water into the Red Sea. Additionally, the Red Sea's elevated temperatures, compared to the Indian Ocean, could result in enhanced evaporation rates. This, in turn, might augment the transfer of water from the Indian Ocean to the Red Sea. However, as the primary supplier of nutrients and trace elements to the Red Sea, the Indian Ocean's rapid warming (and that of the Red Sea) is likely to intensify ocean stratification. This amplified stratification could disrupt the vertical exchanges between the ocean's surface and its deeper, nutrient-rich layers^{9,10,27}. As a result, the nutrient concentration of the water entering the Red Sea might decrease,

Table 2 Average element accumulation rates (EARs) of the Red Sea sediment cores.

Element	South Red Sea sediment core (N = 19)			North Red Sea sediment core (N = 24)		
	Year < 1870	Year > 1870	EAR changes	Year < 1870	Year > 1870	EAR changes
Ca	205 ± 24.4 (a)	168 ± 34.4 (b)	-17.8%	1526 ± 128 (A)	1652 ± 282 (A)	8.29%
Si	144 ± 24.6 (a)	145 ± 32.1 (a)	0.85%	473 ± 51.5 (A)	531 ± 110 (A)	12.4%
Mg	19.3 ± 2.37 (a)	17.6 ± 3.41 (a)	-8.52%	114 ± 9.42 (A)	127 ± 26.2 (A)	12.0%
Na	29.9 ± 2.94 (a)	30.8 ± 4.72 (a)	2.94%	64.1 ± 6.72 (B)	80.4 ± 25.3 (A)	25.4%
Fe	19.3 ± 3.38 (a)	18.9 ± 4.21 (a)	-1.82%	73.3 ± 9.77 (A)	76.6 ± 16.6 (A)	4.56%
TOC	45.3 ± 5.49 (a)	38.6 ± 8.55 (a)	-14.9%	21.4 ± 2.16 (A)	27.8 ± 16.9 (A)	30.1%
S	7.17 ± 0.82 (a)	5.93 ± 0.98 (b)	-17.2%	28.0 ± 2.37 (A)	31.8 ± 6.02 (A)	13.4%
TN	6.27 ± 0.77 (a)	5.40 ± 1.24 (a)	-14.0%	4.27 ± 0.43 (A)	4.30 ± 0.77 (A)	0.85%
P	1.97 ± 0.22 (a)	1.65 ± 0.33 (b)	-16.4%	5.72 ± 0.55 (A)	6.25 ± 1.31 (A)	9.29%
Zn	0.080 ± 0.011 (a)	0.077 ± 0.016 (a)	-3.76%	0.33 ± 0.035 (A)	0.38 ± 0.081 (A)	13.8%
V	0.16 ± 0.035 (a)	0.12 ± 0.039 (b)	-25.8%	0.17 ± 0.021 (A)	0.20 ± 0.042 (A)	12.6%
Ni	0.058 ± 0.0064 (a)	0.052 ± 0.011 (a)	-10.30%	0.14 ± 0.019 (B)	0.17 ± 0.034 (A)	19.5%
Cr	0.054 ± 0.0073 (a)	0.049 ± 0.011 (a)	-9.24%	0.12 ± 0.013 (B)	0.14 ± 0.030 (A)	17.6%
Cu	0.033 ± 0.0046 (a)	0.031 ± 0.0069 (a)	-6.85%	0.10 ± 0.014 (A)	0.12 ± 0.029 (A)	14.4%
Cd	0.0033 ± 0.00072 (a)	0.0025 ± 0.00067 (b)	-23.0%	0.0056 ± 0.00057 (A)	0.0061 ± 0.0013 (A)	8.69%

TOC total organic carbon, TN total nitrogen.
 Notes: EAR: Mean ± standard deviation, $\mu\text{g cm}^{-2} \text{decade}^{-1}$, dry-weight basis) and their relative changes in the South and North Red Sea sediment cores before and after the 1870s. The relative changes of the EAR = $[(\text{EAR}_{(\text{years} > 1870)} - \text{EAR}_{(\text{years} < 1870)}) / \text{EAR}_{(\text{years} < 1870)}] * 100\%$. Data in the same row marked with different lower or uppercase letters are significantly different ($p < 0.05$).

Table 3 Linear regression slopes between the element accumulation rates (EAR, $\mu\text{g cm}^{-2} \text{decade}^{-1}$) and years, and the rate of change in the slope before and after the 1870s for the Red Sea sediment cores.

Element	South Red Sea sediment core (N = 19)			North Red Sea sediment core (N = 24)		
	Year < 1870	Year > 1870	Slope change & EAR change tendency	Year < 1870	Year > 1870	Slope change & EAR change tendency
TOC	-2.18×10^0	-8.27×10^0	-279%, decreased	-4.71×10^{-1}	2.48×10^1	5357%, increased
TN	-2.70×10^{-1}	-1.06×10^0	-293%, decreased	-2.66×10^{-1}	1.20×10^0 *	552%, increased
Na	-7.25×10^{-1}	-2.03×10^0	-180%, decreased	2.38×10^0	$3.85 \times 10^{1**}$	1516%, increased
Mg	1.99×10^{-2}	-2.76×10^0	-13,980%, decreased	-4.43×10^0	2.89×10^1	752%, increased
Si	1.26×10^1	-3.34×10^1	-364%, decreased	-2.27×10^1	1.13×10^2	598%, increased
P	$-1.87 \times 10^{-1*}$	-1.13×10^{-1}	+40.0%, decreased	$-4.80 \times 10^{-1*}$	1.54×10^0	420%, increased
S	-5.76×10^{-1}	-5.55×10^{-1}	+4.00%, decreased	-3.34×10^{-1}	6.30×10^0	1988%, increased
Ca	-1.46×10^1	-2.67×10^1	-83.0%, decreased	-4.75×10^1	2.02×10^2	525%, increased
V	3.05×10^{-3}	$-5.90 \times 10^{-2*}$	-2034%, decreased	$-1.79 \times 10^{-2*}$	$5.26 \times 10^{-2*}$	394%, increased
Cr	2.85×10^{-3}	-1.00×10^{-2}	-452%, decreased	-4.53×10^{-3}	3.17×10^{-2}	800%, increased
Fe	2.18×10^0	-3.90×10^0	-279%, decreased	-8.73×10^0 *	$2.03 \times 10^{1*}$	332%, increased
Ni	6.44×10^{-4}	-9.86×10^{-3}	-1631%, decreased	6.81×10^{-3}	5.29×10^{-3}	-22.0%, increased
Cu	1.80×10^{-3}	-7.54×10^{-3}	-519%, decreased	-3.98×10^{-3}	$3.59 \times 10^{-2*}$	1003%, increased
Zn	1.08×10^{-3}	-1.53×10^{-2}	-1514%, decreased	-7.93×10^{-3}	6.38×10^{-2}	905%, increased
Cd	-1.50×10^{-4}	-9.85×10^{-4}	-554%, decreased	$-4.84 \times 10^{-4*}$	1.50×10^{-3}	410%, increased

TOC total organic carbon, TN total nitrogen.
 Notes: EAR slope change rate = $[(\text{slope}_{(\text{years} > 1870)} - \text{slope}_{(\text{years} < 1870)}) / |\text{slope}_{(\text{years} < 1870)}|] * 100\%$, where $|\text{slope}_{(\text{years} < 1870)}|$ is the absolute value of the $\text{slope}_{(\text{years} < 1870)}$. * $p < 0.05$, ** $p < 0.01$.

leading to a potential decline in nutrient inputs. On the other hand, warming is expected to weaken the monsoon winds over the Red Sea and Indian Ocean^{34,35}, potentially impairing the driving force of horizontal exchange of nutrient-rich intermediate water intrusion from the Indian Ocean into the Red Sea that occurs during the summer southwest monsoon.

Anthropogenic activity-driven pollutant accumulation in the Red Sea. Sediment core analysis has provided valuable insight into the temporal increase in element concentrations and their correlation with human activities in Saudi Arabia. The North Red Sea sediment core displayed a significant rise in most measured element concentrations, except for TN and Ca, from the 1930s onwards, as depicted in Fig. 1. The analysis suggested that this increase coincided with the discovery of Saudi Arabia’s first oil field, the Dammam oilfield, in 1938.

Furthermore, we observed a noteworthy increase in the average element accumulation rates of the North Red Sea sediment cores after the 1870s, with a minimum growth rate of 0.85% for TN and a maximum growth rate of 30.1% for TOC (Figs. 2 and 3f and Table 2). The linear regression analysis revealed that the slopes of certain trace metal accumulation rates, including V, Cr, Fe, Cu, Zn, and Cd, experienced a significant surge after the 1870s. The slopes of these element accumulation rates multiplied by 3.94, 8.00, 3.32, 10.03, 9.05, and 4.10 times, respectively (Table 3). Moreover, this study indicated that all measured element accumulation rates experienced a higher rate of increase after the 1970s (Fig. 2), coinciding with Saudi Arabia’s industrialization along the Red Sea’s eastern coast. This period includes the establishment and operation of the Yanbu Industrial City Zone (1975), the Saudi Aramco Lubricating Oil Refining Company (1976), the Yanbu Cement Company (1977), the Yanbu

Commercial Port (expansion in 1979), the Yanbu Industrial Port (1980), the Yanbu Power Plant (1980), the East–West Crude Oil Pipeline (1981), and the Saudi Arabian Oil Company and Mobil Yanbu Refining Company (1981). This finding aligns with the reports by Al-Rousan et al.¹⁴, who noted a substantial increase (ranging from 17% to 300%) in most trace metal concentrations, including Cd, Cu, Mn, Pb, and Zn, in hard corals collected from the North Red Sea since the 1960s.

These data indicate an alarming increase in the accumulation of various elements, including trace metals, in the North Red Sea. This phenomenon is primarily attributed to the rapid expansion of anthropogenic activity in the region over the past 150 years. The shipping activity surge following the opening of the Suez Canal in 1869¹⁷ and the rapid development of oil-related sectors in Saudi Arabia and Egypt, including oil refineries and petrochemical plants¹⁸, notably contributed to this trend. Several other anthropogenic activities have also played a notable role in the accumulation of these elements in the North Red Sea, such as dredging/filling, operation of crude oil terminals/ports, accidental oil spills, deliberate attacks on oil infrastructures³⁶, and the construction and running of high-pollution industries, such as cement factories¹⁵ and power plants that burn crude oil as fuel. The rapid urbanization and massive population boom in coastal cities, such as Jeddah, Rabigh, and Yanbu, exacerbated this situation further. The semi-enclosed structure of the North Red Sea basin, absence of river inputs, rare precipitation, and high seawater evaporation rates^{37,38} limit water exchange in the region, making discharged pollutants more persistent in the aquatic environment. Thus, the biota of the Red Sea is more vulnerable to trace metal pollution.

Red Sea ecosystem prediction. The Red Sea is undergoing rapid warming and facing reduced nutrient supplies from the Indian Ocean in the South. Simultaneously, it is experiencing heightened pollutant levels, including trace metals, from human activities in the North. We propose the term “Cai-Agusti Marine Crisis Conflux (CAMCC)” to describe the confluence of these three stressors. Within this context, it’s evident that these intertwined factors have played a crucial role in sculpting the marine ecosystems of the Red Sea. For instance, ocean warming has caused massive coral bleaching events in the Red Sea^{6,7} due to thermal stress and accumulation of reactive oxygen species³⁹. The increasing ocean stratification caused by ocean warming could also reduce the supply of limited nutrients to the Red Sea^{8,10} and further challenge the coral’s capacity to produce sufficient antioxidant enzymes to resist thermal stress⁴⁰. Moreover, excessively high concentrations of trace metals, such as Cu, can restrain key biological processes in coral and increase energy costs for cellular detoxification and repair⁴¹, contributing to reduced resistance of coral to thermal stress under warming scenarios⁴².

The Cai-Agusti Marine Crisis Conflux (CAMCC) delineates a scenario with intensifying thermal stress, declining nutrient levels, and escalating elemental pollution, especially trace metals. This conflux likely synergizes with other prevailing stressors, such as high ultraviolet B radiation, and newer threats like microplastics. Collectively, these pressures can gravely endanger Red Sea marine life. Potential outcomes include reduced food availability^{8,10}, deterioration of breeding and feeding habitats^{14,16}, amplified species competition, and alterations in marine species abundance, diversity, and distribution⁴³. Ultimately, these combined factors might result in large-scale mortality events⁴⁴, hasten the extinction of specific species⁴⁵, and degrade the overall marine ecosystems of the Red Sea. In support of this, the Red Sea corals, in regions where seawater temperatures have risen by about 0.4 to 1 °C since the mid-1970s, exhibited a 30% decrease in skeletal

extension and an 18% reduction in calcification rates between 1998 and 2010⁴⁶. Simultaneously, corroborating this trend, there has been a documented shift towards community homogenization, accompanied by a decrease in the average size of coral colonies in the Red Sea, spanning from 1997 to 2009⁴⁷.

In conclusion, the unique environment of the Red Sea presents a rare chance to assess and foresee the implications of global warming and anthropogenic activities on marine ecosystems. The ramifications of these stressors, highlighted by the Cai-Agusti Marine Crisis Conflux (CAMCC) we’ve proposed in this research, could echo well beyond the confines of the Red Sea, influencing marine ecosystems worldwide. Thus, we call for urgent actions to reduce global greenhouse gas emissions, aiming to counteract ocean warming. In addition, we stress the importance of embracing cleaner technologies to minimize pollutants from local anthropogenic activities. Undertaking these proactive initiatives is pivotal to both preserving the Red Sea’s rich biodiversity and preempting analogous ecological challenges in marine environments across the globe.

Methods

Study area and sampling methods. This study collected two sediment cores from the South and North Red Sea. The first core, located at (17.33° N, 41.39° E) and retrieved from a water column depth of 390 m, measures 20 cm in length with an inner diameter of 8.6 cm. It was obtained using a gravity corer from the South Red Sea in November 2016. The second core, situated at (27.56° N, 35.28° E) and derived from a water column depth of 1050 m, has a length of 18 cm and an inner diameter of 8.6 cm. This core was sampled using a box corer from the North Red Sea in October 2016 (Supplementary Fig. 2). Different corers were used for sampling primarily because these cores were retrieved during two separate cruises with close dates. Managing to have the same coring instrument for both expeditions posed logistical challenges. It’s worth mentioning that our sampling stations, positioned in the open Red Sea, lie more than 23 km away from the nearest coastline, ensuring they remain unaffected by direct human activities.

After collection, the sediment cores were sliced into segments 0.5 cm thick using a plastic knife on board the research vessel and stored in plastic bags at -20 °C for preservation. Once in the laboratory, the samples were transferred into 50 mL centrifuge tubes and freeze-dried for at least 24 h to a constant weight. The samples were homogeneously vortexed for laboratory analysis. Clean techniques were strictly followed throughout the sampling and laboratory work to avoid possible metal contamination, including wearing disposable nitrile gloves, performing a two-person sample collection procedure (clean/dirty hands standard operating procedure), and using ultra-clean (acid-washed) sample collection/digestion containers.

Sediment chronology analysis with ²¹⁰Pb and ¹⁴C. Alpha spectrometry was applied to measure the activity concentrations of ²¹⁰Pb in the upper 0 to 10 cm of the sediment cores. An acid attack using a microwave was performed on the sediment samples⁴⁸. Subsequently, ²¹⁰Po was measured, assuming radioactive equilibrium between both radionuclides. The chronological age of each sediment core segment was determined using the constant flux: constant sedimentation model⁴⁹ and the constant rate of supply model⁵⁰. We utilized the ²¹⁰Pb dating technique for surficial sediment cores primarily due to its stability against human-induced alterations. Notably, atomic bomb activities released surplus ¹⁴C into the environment, which can distort ¹⁴C analysis results for surficial sediments. However, the presence of

^{210}Pb typically wanes around the 10 cm depth in sediments, constraining its use for dating deeper sedimentary sections.

To address this limitation, the nonsurface Red Sea sediment core segments (depth >10 cm) were analyzed using the ^{14}C dating technique. This technique employed accelerator mass spectrometry in the Mini radioCarbon Dating System⁵¹. The system, powered by a 200 kV tandem, is commercialized by the Swiss company Ionplus and adheres to the ISO 17025 and 9001 standard procedures⁵². The raw radiocarbon dates underwent calibration using the R software package “Bacon” for Bayesian chronology building⁵³.

During the realization of this study, analyses of reagent blanks, replicates, and the standard reference material (e.g., International Atomic Energy Agency marine soil samples - IAEA-315 for ^{210}Pb analysis) were conducted in each batch of samples to assess for any contamination and ensure reproducibility of the results.

Total organic carbon and total nitrogen analysis. In this study, the CHNS organic element analyzer (Flash 2000, Thermo Fisher Scientific, USA) was used to analyze the TOC and TN content of the Red Sea sediment samples¹⁵. Specifically, 10 mg of freeze-dried samples were placed in silver capsules (Organic Elemental Analysis Labs Company, UK). These samples were then subjected to acid digestion using increasing volumes (10, 20, 30, 40, and 50 μL) of 3 mol L^{-1} HCl (Fisher Chemical, USA). Each digestion step was conducted at 60 °C for 10 minutes. Prior to analysis, standard curves for TOC and TN concentrations were constructed using 2,5-Bis(5-tert-butyl-2-benzo-oxazol-2-yl) thiophene ($\text{C}_{26}\text{H}_{26}\text{N}_2\text{O}_2\text{S}$, Thermo Fisher Scientific, USA) at concentrations of 2, 4, 6, 8, and 10 mg, demonstrating a high degree of correlation (R -values > 0.997). Following digestion, the silver capsules for each sample were carefully wrapped into balls and placed in tin capsules (Organic Elemental Analysis Labs Company, UK) for analysis. silver and tin capsule without a sample was wrapped into a ball and analyzed using the instrument as the sample blank.

Element analysis and element accumulation rate calculation. 50-mg freeze-dried sediment samples were digested using an acid mixture (6 mL of 69% HNO_3 and 2 mL of 30% H_2O_2 , Fisher Chemical, USA) via a microwave digestion system (single reaction chamber microwave digestion system, Milestone Technologies, USA). The samples were first digested at 130 °C and 10 MPa (100 bar, 98.69 standard atmospheric pressure) for 10 min and then redigested at 240 °C and 10 MPa for another 25 min. After cooling, the sample solutions were diluted to 25 mL using Milli-Q distilled water and analyzed using Inductively coupled plasma-optical emission spectrometry (ICP-OES, Model: 5110, Agilent Technologies, USA)⁵⁴.

The Na, Mg, P, S, and Ca concentrations were measured separately against V, Cr, Fe, Ni, Cu, Zn, and Cd concentrations to mitigate potential systematic error or interference effects. The calibration curves of the measured element standard solutions (0.1, 1, 10, and 100 $\mu\text{g L}^{-1}$) displayed correlation coefficients (R values) greater than 0.999. The limit of detection, quantitation, and practical quantitation limits for the mentioned elements were less than 0.019, 0.063, and 0.16 mg kg^{-1} , respectively. Three replicates of 50 mg standard reference material (SRM) of inorganics in marine sediment (SRM 2702, National Institute of Standards and Technology, USA) and sediment for solid sampling (SRM 2703) were also analyzed alongside the sediment samples to verify data validity and the precision/accuracy of the analytical methods. A series of quality control procedures were strictly followed: running continuous calibration verification standard solutions, laboratory fortified blanks (same as acid or

sample blanks), laboratory reagent blanks (acid blanks spiked with standard element solutions), quality control standards, and duplicated samples spiked with quality control standard solutions to ensure the reliability of the ICP-OES instrument. The recovery rates for all these quality control procedures ranged from 90% to 110%, whereas the measured element concentrations of the standard reference materials were consistent with the reference concentrations (78.91–119.57%; Supplementary Tables 2–3).

The EARs ($\mu\text{g cm}^{-2} \text{ decade}^{-1}$, dry-weight basis) in sediments were used to study environmental changes, reconstruct past conditions, and identify pollution sources⁵⁵. The EARs at different vertical depths (or different chronological ages) of the Red Sea sediment cores were calculated using the following modified equations⁵⁶:

$$\text{EAR} = \text{EC}(\mu\text{g g}^{-1}) \times \text{Dry Bulk Density}(\text{g cm}^{-3}) \times \text{SR}(\text{cm decade}^{-1}) \quad (1)$$

$$\text{SR} = \frac{\text{Depth at year Y}(\text{cm}) - \text{Depth at year X}(\text{cm})}{(\text{Year X} - \text{Y}) \times 10} \quad (2)$$

where EC and SR are the element concentration and sedimentation rate of the Red Sea sediment cores, respectively. The sediment dry bulk density was calculated as the mass of dry solids in a given volume of sediment (Supplementary Data 1). The relative changes of the sediment EAR before and after the 1870s were calculated using the following equation:

$$\text{Relative changes of EAR} = \frac{[\text{EAR}_{(\text{years}>1870)} - \text{EAR}_{(\text{years}<1870)}] * 100\%}{\text{EAR}_{(\text{years}<1870)}} \quad (3)$$

To analyze the relationship between sediment EAR and chronological age, a linear regression analysis was employed to determine the slopes of the regression lines. The calculation of the EAR slope change rates before and after the 1870s was conducted using the following equation:

$$\text{EAR slope change rate} = \frac{[\text{Slope}_{(\text{years}>1870)} - \text{Slope}_{(\text{years}<1870)}] * 100\%}{|\text{Slope}_{(\text{years}<1870)}|} \quad (4)$$

where $|\text{Slope}_{(\text{years}<1870)}|$ is the absolute value of the slope $_{(\text{years}<1870)}$.

Silica analysis. The Si sediment concentrations were not measured using ICP-OES due to the inability of nitric acids to dissolve the silicate compounds in the sediment samples. Although hydrofluoric acid can dissolve the silicate compounds of the sediment samples, its use poses considerable safety risks and can cause damage to the glassy components of the ICP-OES instrument (such as the pneumatic nebulizer). Instead, the Si concentrations in the sediment samples were assessed using an X-ray fluorescence spectrometer (Model: XGT-7000, HORIBA Scientific, Canada). 10 mg of 12 sediment samples were weighed and evenly spread on the instrument's sample holder. The instrument selected four measuring points for each sample and scanned these points for 300 s. After that, the integrated software calculated the peak area and corresponding Si concentration for each measuring point⁵⁷.

Statistical analysis. The differences in element concentrations between the South and North Red Sea sediment core were analyzed using one-way analysis of variance or two independent sample nonparametric tests in the SPSS statistical analysis software (Version 27.0, IBM Corporation, USA), based on the homogeneity of variance. The linear regression analysis was employed to calculate the slopes of the regression lines between the chronological age and EARs of the Red Sea sediment cores. Multivariate correlation analysis was conducted using OriginPro

software (Version 2022, OriginLab Corporation, USA) to investigate Pearson correlations within or between the years (chronological age), element concentrations, and EARs of the sediment cores. Statistical significance was defined as a p value < 0.05 .

Reporting summary. Further information on research design is available in the Nature Portfolio Reporting Summary linked to this article.

Data availability

The supplementary dataset utilized for this study can be accessed on Figshare at the following link: <https://doi.org/10.6084/m9.figshare.24279262.v2>.

Received: 2 July 2023; Accepted: 10 November 2023;

Published online: 20 November 2023

References

- Zalasiewicz, J. et al. The Working Group on the Anthropocene: Summary of evidence and interim recommendations. *Anthropocene* **19**, 55–60 (2017).
- Burke, A. et al. The archaeology of climate change: The case for cultural diversity. *Proc. Natl. Acad. Sci. USA* **118**, 10 (2021).
- Raitsos, D. E., Pradhan, Y., Brewin, R. J. W., Stenchikov, G. & Hoteit, I. Remote Sensing the Phytoplankton Seasonal Succession of the Red Sea. *Plos One* **8**, 9 (2013).
- Chaidez, V., Dreano, D., Agusti, S., Duarte, C. M. & Hoteit, I. Decadal trends in Red Sea maximum surface temperature. *Sci. Rep.* **7**, 8 (2017).
- Raitsos, D. E. et al. Abrupt warming of the Red Sea. *Geophys. Res. Lett.* **38**, 5 (2011).
- Furby, K. A., Bouwmeester, J. & Berumen, M. L. Susceptibility of central Red Sea corals during a major bleaching event. *Coral Reefs* **32**, 505–513 (2013).
- Monroe, A. A. et al. In situ observations of coral bleaching in the central Saudi Arabian Red Sea during the 2015/2016 global coral bleaching event. *PLoS One* **13**, e0195814 (2018).
- Behrenfeld, M. J. et al. Climate-driven trends in contemporary ocean productivity. *Nature* **444**, 752–755 (2006).
- Coma, R. et al. Global warming-enhanced stratification and mass mortality events in the Mediterranean. *Proc. Natl. Acad. Sci. USA* **106**, 6176–6181 (2009).
- Li, G. C. et al. Increasing ocean stratification over the past half-century. *Nat. Clim. Chan.* **10**, 1116–U1176 (2020).
- Schulhof, M. A., Shurin, J. B., Declerck, S. A. J. & Van de Waal, D. B. Phytoplankton growth and stoichiometric responses to warming, nutrient addition and grazing depend on lake productivity and cell size. *Global Chan. Biol.* **25**, 2751–2762 (2019).
- Churchill, J. H., Bower, A. S., McCorkle, D. C. & Abualnaja, Y. The transport of nutrient-rich Indian Ocean water through the Red Sea and into coastal reef systems. *J. Marine Res.* **72**, 165–181 (2014).
- Raitsos, D. E. et al. Monsoon oscillations regulate fertility of the Red Sea. *Geophys. Res. Lett.* **42**, 855–862 (2015).
- Al-Rousan, S. A., Al-Shioul, R. N., Al-Horani, F. A. & Abu-Hilal, A. H. Heavy metal contents in growth bands of Porites corals: Record of anthropogenic and human developments from the Jordanian Gulf of Aqaba. *Marine Pollut. Bull.* **54**, 1912–1922 (2007).
- Cai, C. Z., Devassy, R. P., El-Sherbiny, M. M. & Agusti, S. Cement and oil refining industries as the predominant sources of trace metal pollution in the Red Sea: A systematic study of element concentrations in the Red Sea zooplankton. *Marine Pollut. Bull.* **174**, 11 (2022).
- Nour, H. E. & Noub, E. Using coral skeletons for monitoring of heavy metals pollution in the Red Sea Coast, Egypt. *Arabian J. Geosci.* **13**, 12 (2020).
- Barry M. E., Houdre M., McAlister A. B., & Botelho D. A. Three Dimensional Hydraulic and Water Quality Modelling of the Red Sea: Challenges and Learnings. In: *Combined IMACS World Congress/Modelling and Simulation Society-of-Australia-and-New-Zealand (MSSANZ)/18th Biennial Conference on Modelling and Simulation*. Univ Western Australia (2009).
- Kostianaia E. A., Kostianoy A., Lavrova O. Y., & Soloviev D. M. Oil Pollution in the Northern Red Sea: A Threat to the Marine Environment and Tourism Development. In: *Environmental Remote Sensing in Egypt* (eds Elbeih S. F., Negr A. M., Kostianoy A.). Springer International Publishing (2020).
- Morelli, G., Gasparon, M., Fierro, D., Hu, W. P. & Zawadzki, A. Historical trends in trace metal and sediment accumulation in intertidal sediments of Moreton Bay, southeast Queensland, Australia. *Chem. Geol.* **300**, 152–164 (2012).
- Al-Mur, B. A., Quicksall, A. N. & Al-Ansari, A. M. A. Spatial and temporal distribution of heavy metals in coastal core sediments from the Red Sea, Saudi Arabia. *Oceanologia* **59**, 262–270 (2017).
- Badr, N. B. E., El-Fiky, A. A., Mostafa, A. R. & Al-Mur, B. A. Metal pollution records in core sediments of some Red Sea coastal areas, Kingdom of Saudi Arabia. *Environ. Monitor. Assess.* **155**, 509–526 (2009).
- Mannaa, A. A., Khan, A. A., Haredy, R. & Al-Zubieri, A. G. Contamination Evaluation of Heavy Metals in a Sediment Core from the Al-Salam Lagoon, Jeddah Coast, Saudi Arabia. *J. Marine Sci. Engineer.* **9**, 17 (2021).
- Youssef, M., El-Sorogy, A., Osman, M., Ghandour, I. & Manaa, A. Distribution and metal contamination in core sediments from the North Al-Wajh area, Red Sea, Saudi Arabia. *Marine Pollut. Bull.* **152**, 9 (2020).
- Bruland, K. W. OCEANOGRAPHIC DISTRIBUTIONS OF CADMIUM, ZINC, NICKEL, AND COPPER IN THE NORTH PACIFIC. *Earth Planet. Sci. Lett.* **47**, 176–198 (1980).
- Morley, N. H., Statham, P. J. & Burton, J. D. Dissolved Trace-Metals In The Southwestern Indian-Ocean. *Deep-Sea Res Part I-Oceanogr Res. Pap* **40**, 1043–1062 (1993).
- Price, N. M. & Morel, F. M. M. Cadmium And Cobalt Substitution For Zinc In A Marine Diatom. *Nature* **344**, 658–660 (1990).
- Roxy, M. K. et al. A reduction in marine primary productivity driven by rapid warming over the tropical Indian Ocean. *Geophys. Res. Lett.* **43**, 826–833 (2016).
- Webster P., Gullede J., & Curry J. Expanding tropical warm pool: increased tropical cyclone season length and storm duration. In: *AGU Fall Meeting Abstracts* (2006).
- Lashof, D. A. & Ahuja, D. R. Relative Contributions Of Greenhouse Gas Emissions To Global Warming. *Nature* **344**, 529–531 (1990).
- Saager, P. M., Debaar, H. J. W. & Howland, R. J. CD, ZN, NI And CU In The Indian-Ocean. *Deep-Sea Res. Part a-Oceanograph. Res. Papers* **39**, 9–35 (1992).
- Inoue M., Suzuki A., Nohara M., Hibino K., & Kawahata H. Empirical assessment of coral Sr/Ca and Mg/Ca ratios as climate proxies using colonies grown at different temperatures. *Geophys. Res. Lett.* **34**, L12611, (2007).
- McConnell M. C., & Thunell R. C. Calibration of the planktonic foraminiferal Mg/Ca paleothermometer: Sediment trap results from the Guaymas Basin, Gulf of California. *Paleoceanography* **20**, PA2016, (2005).
- Marcott, S. A., Shakun, J. D., Clark, P. U. & Mix, A. C. A Reconstruction of Regional and Global Temperature for the Past 11,300 Years. *Science* **339**, 1198–1201 (2013).
- Rao, S. A. et al. Why is Indian Ocean warming consistently? *Clim. Chan.* **110**, 709–719 (2012).
- Swapna, P., Krishnan, R. & Wallace, J. M. Indian Ocean and monsoon coupled interactions in a warming environment. *Clim. Dynam.* **42**, 2439–2454 (2014).
- Huynh, B. Q. et al. Public health impacts of an imminent Red Sea oil spill. *Nat. Sustain.* **4**, 1084–1091 (2021).
- Sofianos S., & Johns W. E. Water Mass Formation, Overturning Circulation, and the Exchange of the Red Sea with the Adjacent Basins. In: *The Red Sea: The Formation, Morphology, Oceanography and Environment of a Young Ocean Basin* (eds Rasul N. M. A., Stewart I. C. F.). (Springer Berlin Heidelberg, 2015).
- Sofianos, S. S., Johns, W. E. & Murray, S. P. Heat and freshwater budgets in the Red Sea from direct observations at Bab el Mandeb. *Deep-Sea Res Part II-Top Stud Oceanogr* **49**, 1323–1340 (2002).
- El-Orabi, N. F., Rogers, C. B., Edwards, H. G. & Schwartz, D. D. Heat-induced inhibition of superoxide dismutase and accumulation of reactive oxygen species leads to HT-22 neuronal cell death. *J. Thermal Biol* **36**, 49–56 (2011).
- Ferrier-Pages, C., Sauzeat, L. & Balter, V. Coral bleaching is linked to the capacity of the animal host to supply essential metals to the symbionts. *Global Chan. Biol.* **24**, 3145–3157 (2018).
- da Silva, E. S., Abril, S. I. M., Zanette, J. & Bianchini, A. Salinity-dependent copper accumulation in the guppy *Poecilia vivipara* is associated with CTR1 and ATP7B transcriptional regulation. *Aquatic Toxicol.* **152**, 300–307 (2014).
- Banc-Prandi, G. & Fine, M. Copper enrichment reduces thermal tolerance of the highly resistant Red Sea coral *Stylophora pistillata*. *Coral Reefs* **38**, 285–296 (2019).
- Jiang, L. & Morin, P. J. Temperature-dependent interactions explain unexpected responses to environmental warming in communities of competitors. *J. Animal Ecol.* **73**, 569–576 (2004).
- Genin, A., Levy, L., Sharon, G., Raitsos, D. E. & Diamant, A. Rapid onsets of warming events trigger mass mortality of coral reef fish. *Proc. Natl. Acad. Sci. USA* **117**, 25378–25385 (2020).
- Traill, L. W., Lim, M. L. M., Sodhi, N. S. & Bradshaw, C. J. A. Mechanisms driving change: altered species interactions and ecosystem function through global warming. *J. Animal Ecol.* **79**, 937–947 (2010).

46. Cantin, N. E., Cohen, A. L., Karnauskas, K. B., Tarrant, A. M. & McCorkle, D. C. Ocean warming slows coral growth in the central Red Sea. *Science* **329**, 322–325 (2010).
47. Riegl, B. M., Bruckner, A. W., Rowlands, G. P., Purkis, S. J. & Renaud, P. Red Sea coral reef trajectories over 2 decades suggest increasing community homogenization and decline in coral size. *PLoS One* **7**, e38396 (2012).
48. Sanchez-Cabeza, J. A., Masque, P. & Ani-Ragolta, I. Pb-210 and Po-210 analysis in sediments and soils by microwave acid digestion. *J. Radioanal. Nuclear Chem.* **227**, 19–22 (1998).
49. Krishnaswamy, S., Lal, D., Martin, J. M. & Meybeck, M. Geochronology of lake sediments. *Earth Planet. Sci. Lett.* **11**, 407–414 (1971).
50. Appleby, P. G. & Oldfieldz, F. The assessment of 210Pb data from sites with varying sediment accumulation rates. *Hydrobiologia* **103**, 29–35 (1983).
51. Synal, H. A., Stocker, M. & Suter, M. MICADAS: A new compact radiocarbon AMS system. *Nuclear Instr. Methods Phys. Res. Section B-Beam Interact. Mater. Atoms* **259**, 7–13 (2007).
52. Saderne, V. et al. Accumulation of Carbonates Contributes to Coastal Vegetated Ecosystems Keeping Pace With Sea Level Rise in an Arid Region (Arabian Peninsula). *J. Geophys. Res.-Biogeosci* **123**, 1498–1510 (2018).
53. Blaauw, M. & Christen, J. A. Flexible Paleoclimate Age-Depth Models Using an Autoregressive Gamma Process. *Bayesian Anal.* **6**, 457–474 (2011).
54. Mokoena, D. P., Mngadi, S. V. & Nomngongo, P. N. Microwave-Assisted Extraction of Trace Metals from Sediments using Dilute Hydrogen Peroxide and Dilute Nitric Acid Prior to their Determination by Inductively Couple Plasma-Optical Emission Spectrometry. *Curr. Anal. Chem.* **16**, 970–978 (2020).
55. Ruiz-Fernandez, A. C. et al. Historical reconstruction of sediment accumulation rates as an indicator of global change impacts in a tropical crater lake. *J. Paleolimnol.* **68**, 395–413 (2022).
56. McMurtry, G. M., Veeh, H. H. & Moser, C. Sediment Accumulation Rate Patterns On The Northwest Nazca Plate. *Geological Soc. Am. Memoirs* **154**, 211–249 (1981).
57. Reidinger, S., Ramsey, M. H. & Hartley, S. E. Rapid and accurate analyses of silicon and phosphorus in plants using a portable X-ray fluorescence spectrometer. *New Phytol.* **195**, 699–706 (2012).

Acknowledgements

This publication's research was supported by the King Abdullah University of Science and Technology (KAUST) through funding provided to Susana Agusti (BAS/1/1072-01-01) and the Red Sea Research Center. We extend our gratitude to the Coastal & Marine Resources Core Lab (CMOR) staff of King Abdullah University of Science and Technology (KAUST) for their invaluable assistance in deploying the sampling instruments.

Additionally, we thank Jordi Garcia Orellana for conducting the chronology analyses, Vijayalaxmi Dasari for her help with laboratory analyses, and Yixin Wang for offering insightful suggestions on physical oceanography.

Author contributions

S.A. conceptualized and outlined the analytical approach. C.C. performed the element analysis and wrote the manuscript. A.D. performed the sediment chronology analysis. All authors participated in reviewing and refining the manuscript.

Competing interests

The authors declare no competing interests.

Additional information

Supplementary information The online version contains supplementary material available at <https://doi.org/10.1038/s43247-023-01097-6>.

Correspondence and requests for materials should be addressed to Chunzhi Cai.

Peer review information *Communications Earth & Environment* thanks Jibiao Zhang and the other, anonymous, reviewer(s) for their contribution to the peer review of this work. Primary Handling Editors: Clare Davis. A peer review file is available.

Reprints and permission information is available at <http://www.nature.com/reprints>

Publisher's note Springer Nature remains neutral with regard to jurisdictional claims in published maps and institutional affiliations.



Open Access This article is licensed under a Creative Commons Attribution 4.0 International License, which permits use, sharing, adaptation, distribution and reproduction in any medium or format, as long as you give appropriate credit to the original author(s) and the source, provide a link to the Creative Commons license, and indicate if changes were made. The images or other third party material in this article are included in the article's Creative Commons license, unless indicated otherwise in a credit line to the material. If material is not included in the article's Creative Commons license and your intended use is not permitted by statutory regulation or exceeds the permitted use, you will need to obtain permission directly from the copyright holder. To view a copy of this license, visit <http://creativecommons.org/licenses/by/4.0/>.

© The Author(s) 2023